ELSEVIER

Journal of Chromatography A, 930 (2001) 79–93

JOURNAL OF CHROMATOGRAPHY A

www.elsevier.com/locate/chroma

Protein adsorption on novel acrylamido-based polymeric ion-exchangers
III. Salt concentration effects and elution behavior

A.K. Hunter, G. Carta*

Department of Chemical Engineering, University of Virginia, Charlottesville, VA 22903-2442, USA

Received 18 April 2001; received in revised form 27 July 2001; accepted 27 July 2001

Abstract

The effect of salt concentration on the adsorption and desorption of BSA has been determined for a polymeric anion-exchanger based on acrylamido monomers. The material investigated possesses a high adsorption capacity at low salt concentration and the bound protein can be recovered quantitatively at high salt concentrations. The effects of salt on adsorption and desorption rates were evaluated from batch and shallow-bed experiments, and a model was developed to describe the data quantitatively. The adsorption capacity decreases as the salt concentration is increased, but both adsorption and desorption rates increase at higher salt concentrations. The predictability of the behavior of columns packed with this material was examined by comparing model predictions and experimental results obtained in laboratory columns. In general, a good agreement was obtained between predicted and experimental breakthrough and elution profiles, especially in shorter columns. Thus, the model allows a prediction of the effects of column length, mobile phase flow-rate, protein feed concentration, and salt concentration on dynamic capacity, productivity, and on the concentration of product fractions.

Keywords: Salt effects; Ion exchangers; Polymeric gels; Retention behaviour; Diffusion; Proteins; Acrylamido monomers

1. Introduction

In recent years there has been a growing interest in modeling mass transfer in protein ion-exchange media, and in particular those used in capture applications. As pointed out by Lightfoot [1], capture from dilute solutions is often the bottleneck in the overall separation train. Thus, optimizing this step can yield significant reductions in both capital investment and processing time. A quantitative description of the transport phenomena in such processes is critical if one hopes to achieve optimal design.

Although prior work in this area has emphasized modeling the adsorption step (e.g., Refs. [2–8]), the rate at which desorption of the bound protein occurs is also important since the productivity is dependent on the total cycle time. With ion-exchangers, a high salt concentration is typically used elute the protein [9,10]. For these conditions, intraparticle mass transfer tends to be limiting. Thus, an understanding of the related mass transfer effects is of both fundamental and practical value. In the past, relatively few studies have addressed this issue. Graham and Fook [11] investigated the adsorption–desorption of BSA

*Corresponding author. Tel.: +1-434-924-6281; fax: +1-434-982-2658.

E-mail address: gc@virginia.edu (G. Carta).

0021-9673/01/$ – see front matter
PII: S0021-9673(01)01162-1

on a cellulose-based DEAE resin. They found that the initial rate of desorption was much faster than one would predict based on adsorption experiments, and hypothesized that a substantial amount of protein was bound at the outer surface of the particle and did not encounter internal diffusional resistance during desorption. Tsou and Graham [12] studied adsorption and desorption of BSA on a dextran-based ion-exchanger. Their resin showed large volume changes as the salt concentration was varied and they modeled this effect by including a ''protein exclusion term'' in the mass balance equations. Lewus et al. [13] examined the adsorption and desorption of a protein from gel-filled rigid particles at different salt concentrations. They found that adsorption kinetics did not change substantially as the salt concentration was increased. However, desorption rates were approximately three times faster at high salt concentrations. Conder and Hayek [14] investigated the adsorption and desorption kinetics of BSA on a weak anion-exchanger. However, their study was limited in scope to experiments where adsorption and desorption were conducted at the same salt concentration. Thus, desorption occurred very slowly, being limited by the favorable nature of the adsorption isotherm. Finally, Lewus and Carta [15] examined the adsorption and desorption kinetics of cytochrome c in charged polyacrylamide gels immobilized in fused-silica capillaries. Their findings also indicated that desorption rates at high salt concentrations were greater than adsorption rates at low salt concentration.

In our recent work [16,17] we have focused on the characterization of the low-ionic-strength adsorptive properties (equilibrium and mass transfer) of a novel experimental acrylamido-based ion-exchanger for protein chromatography known as BRX-Q. This material showed a large equilibrium uptake capacity at low salt concentrations (280 mg BSA/ml) and high rates of mass transfer. As a result, the dynamic capacity of columns packed with BRX-Q was found to exceed 100 mg BSA/ml column volume, even in columns as short as 1.5 cm operated at 1000 cm/h. The performance characteristics of BRX-Q were attributed to its unique structure, which was shown to comprise a low-density gel phase interspersed with denser polymeric aggregates. The high density of ionogenic groups in BRX-Q provides a large driving force for mass transfer and a high equilibrium capacity yielding very favorable dynamic capacities.

In this work we examine the adsorption and desorption kinetics of BSA on BRX-Q at different salt concentrations. First, the pore structure of BRX-Q at high salt concentration is probed by inverse size exclusion chromatography. Second, adsorption–desorption kinetics experiments are conducted using both a shallow-bed apparatus and an agitated contactor. Third, the experimental data are used to formulate a model in order to predict the adsorption–desorption behavior of packed columns and assess the effect of mobile phase flow-rate on productivity.

2. Materials

BRX-Q samples were obtained from Bio-Rad Laboratories (Hercules, CA, USA). This material is a strong anion-exchanger based on water-soluble, hydrophilic and vinylic monomers polymerized to yield spherical particles. The anion-exchange functionality derives from the use of a monomer possessing a quaternary ammonium ion group. Thus, no post-polymerization derivatization is necessary since the ionogenic monomer is incorporated directly in the final product [16]. A version of BRX-Q with substantially similar structure and properties has recently become available commercially from Bio-Rad Laboratories and is marketed under the trade name UNOSphere Q. The physical properties of BRX-Q, including particle size distribution, apparent and skeletal densities, ion-exchange capacity, scanning electron microscopy of dried beads, and transmission electron microscopy of thin sections of resin-embedded beads, are given in Ref. [16]. The mean particle diameter for the material used in this work is 89 μm. The samples used in this work were washed in a gravity-fed column with alternating cycles of 500 m*M* NaCl and dilute buffer solutions and stored under refrigeration in buffer.

Bovine serum albumin (BSA, Fraction V powder, Cat. No. A-3912) was obtained from Sigma Chemical Co. (St. Louis, MO, USA) and used without further purification. Dextran T-fractions for size exclusion chromatography (SEC) experiments were obtained from Amersham Pharmacia Biotech (Pis-

cataway, NJ, USA). Other chemicals were obtained from Sigma and from Fisher Scientific (Pittsburgh, PA, USA). All experiments were conducted at room temperature (22±2°C) in a 50 m*M* Tris–HCl buffer at pH 8.5.

3. Methods

3.1. Adsorption isotherms

BSA isotherms were obtained at different salt concentrations from batch adsorption experiments as detailed by Hunter and Carta [16].

3.2. Size exclusion chromatography

SEC experiments were conducted using dextran T-fractions (Pharmacia), glucose, BSA, and NaCl as probe molecules as described by Hunter and Carta [16]. BRX-Q was slurry packed in a 0.5-cm I.D. glass column (Amersham Pharmacia Biotech, Model HR 5/10) in 500 m*M* NaCl. The packed bed length was 10 cm and the mobile phase flow-rate was 0.25 ml/min. A Waters Model R401 differential refractive index detector was used with dextran, glucose, and NaCl samples while a Waters Model 484 UV–Vis detector at 280 nm was used for the BSA samples. Corrections were made as described in Hunter and Carta [16] to account for the extra-column volume.

3.3. Stirred-batch experiments

BSA uptake rates were measured at different salt concentrations in an agitated contactor as described in Ref. [17]. In our experiments, we used 0.2-ml samples of BRX-Q media in 100 ml of 1 mg/ml buffered BSA solution at the desired NaCl concentration stirred magnetically at 300 rpm. The solution protein concentration was obtained by circulating a stream through a UV spectrophotometer at 280 nm.

3.4. Shallow-bed experiments

The desorption rates were measured by a shallow-bed method as described by Lewus et al. [13]. In this method, a shallow adsorbent bed is first loaded with a protein solution at low ionic strength, and then exposed to a salt solution. Because of the extremely low contact time, adsorption and desorption can be regarded as if they occurred on a single particle. Thus, the rate of desorption as a function of time can be obtained directly by measuring the protein concentration in the effluent when the bed is exposed to a salt solution. The total amount of protein desorbed at a given time is calculated by integrating the elution peak numerically.

The shallow bed assembly was realized with a Pharmacia HR 5/2 glass column with two adjustable adapters. A 5–10-μl sample of BRX-Q was sandwiched between two 0.75-cm layers of 100 μm PTFE beads. The flow-rates of the protein solution, buffer, and salt eluent were 4 ml/min, which corresponds to a mobile phase velocity of 1200 cm/h and a residence time of 0.02–0.05 s. The protein feed solution was 1 mg/ml BSA and the feed time was 50 min. The rest of the apparatus was as described previously [17]. In our previous work [17], we demonstrated that for these conditions the bed behaves as an ideal, differential contactor. The effluent was monitored by UV at 280 nm.

3.5. Column experiments

Breakthrough and step elution experiments were conducted in 0.5-cm diameter columns (Pharmacia, Models HR 5/2, HR 5/5 and HR 5/10) with bed lengths between 1.75 cm and 10 cm. Two Pharmacia Model P-500 pumps were used to supply feed and eluents and a ProSys Chromatography workstation (BioSepra, Marlborough, MA, USA) was used to monitor conductivity and UV absorbance at 280 nm. The UV detector gave a linear response up to 5 mg/ml BSA. However, since the protein concentrations obtained upon elution with salt were much higher, 0.2-ml fractions were also collected with a Gilson Model 202 fraction collector and analyzed using a Beckman DU-50 spectrophotometer, following appropriate dilutions. In general, there was good agreement between the UV detector and fractions collected in the range of 1–5 mg/ml protein concentration. However, as a result of the finite fraction volume and the sharpness of the elution profiles, only ''fractograms'', rather than continuous curves, could be obtained experimentally at high protein

concentrations. As a consequence, the eluted fractions are generally somewhat less concentrated than the instantaneous concentration values at the column outlet, especially at early times.

4. Results and discussion

4.1. Adsorption isotherms

The equilibrium uptake isotherms of BSA on BRX-Q at different salt concentrations are shown in Fig. 1. As seen in this figure, the isotherms are nearly rectangular at 0 and 50 m*M* NaCl, but become increasingly less favorable as the salt concentration is raised further. Very limited adsorption occurs at salt concentrations higher than 150 m*M* and no protein adsorption could be detected at 500 m*M* NaCl. Solid lines represent Langmuir isotherms fitted to the data according to:

$$q = \frac{q_m bC}{1 + bC} \quad (1)$$

where q_m and b are equilibrium parameters. These parameters were obtained from a nonlinear fit at each salt concentration and are summarized in Table 1.

4.2. Size exclusion chromatography

The result of SEC experiments in Tris buffer and in buffer containing 500 m*M* NaCl are shown in Fig. 2a and b. The dextran T-fractions used have the following approximate average molecular masses: T-10 = 10 000, T-40 = 40 000, T-70 = 70 000, and T-500 = 500 000. As is seen in Fig. 2a, in Tris buffer alone there is little resolution of dextrans larger than

Table 1
Adsorption equilibrium parameters for BSA in 50 m*M* Tris–HCl at pH 8.5

[NaCl] (m*M*)	q_m (mg/ml)	b (ml/mg)
0	280	500
50	210	250
100	116	37.5
150	80	1.80

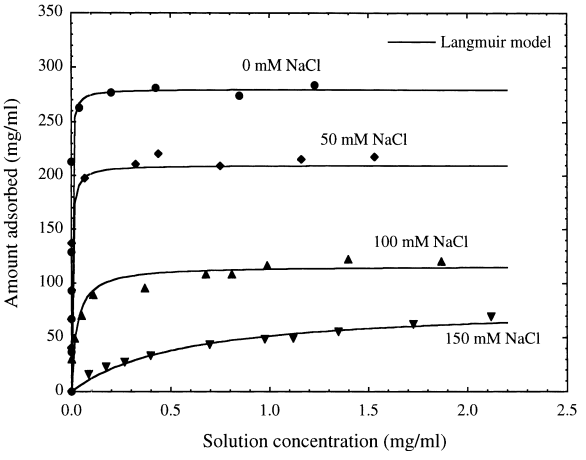

Fig. 1. Adsorption isotherms for BSA on BRX-Q in 50 m*M* Tris–HCl buffer.

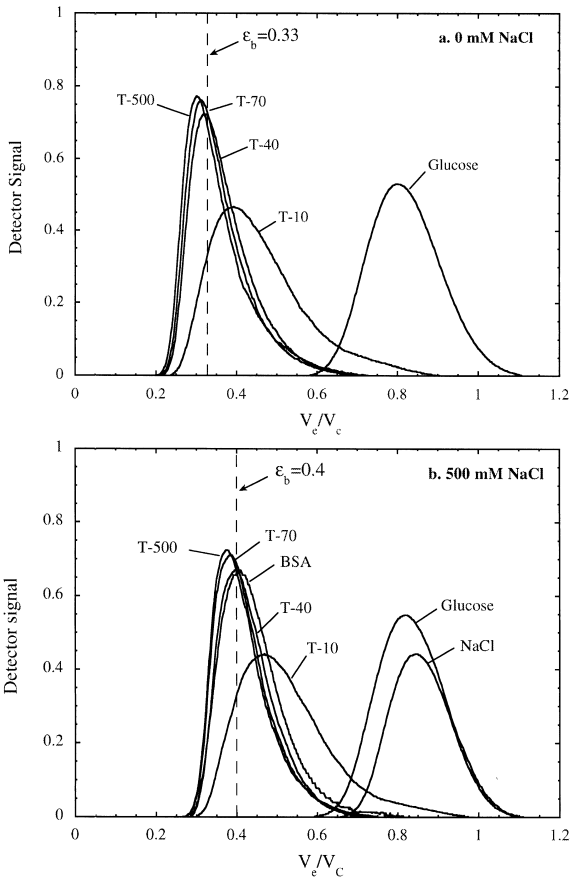

Fig. 2. Size exclusion chromatography peaks for BRX-Q column in 50 m*M* Tris–HCl buffer with (a) 0 m*M* NaCl, (b) 500 m*M* NaCl. Experimental conditions are noted in text.

T-10. An independent determination of the extraparticle void fraction of BRX-Q columns based on pressure drop measurements [16] yielded a value of $\epsilon_b = V_e/V_c \sim 0.33$, which coincides with the retention volume of the larger dextrans. Hence, it appears that dextrans larger than T-40 are nearly completely excluded from the intraparticle space and are eluted in the extraparticle column void volume. The SEC behavior at high salt concentrations does not appear to be significantly different with regards to resolution of the higher molecular mass probes. However, a slight increase in the retention volume of the larger dextrans occurs corresponding to $\epsilon_b = V_e/V_c \sim 0.4$. A slight shrinking of the particles causes this variation. Since the column volume was constant, the particle diameter change can be estimated to be $[(1-0.4)/(1-0.33)]^{1/3} \sim 0.96$, or approximately a 4% decrease. The elution behavior of BSA at 500 m*M* NaCl is also shown in Fig. 2b. At this salt concentration, BSA is unretained and elutes with a retention volume almost identical to that of dextran T-40. Finally, Fig. 2b shows the elution behavior of a NaCl pulse in 500 m*M* NaCl. The retention volume of NaCl ($V_e/V_c \sim 0.85$) is very close to that of glucose ($V_e/V_c \sim 0.82$), indicating that both of these molecules gain access to a large fraction of the intraparticle space.

The chromatographic behavior of these unretained probes is consistent with the structure previously inferred for BRX-Q [16]. This material was shown to comprise a low-density polymer gel interspersed with denser polymer aggregates. In the absence of attractive interactions, the polymer gel excludes almost completely large macromolecules while it allows small molecules such as glucose or NaCl to freely diffuse in the particles. The presence of 500 m*M* NaCl does not appear to alter this behavior significantly and causes only a small particle volume change. The behavior of BSA is especially interesting. At low ionic strength, this species is strongly bound to BRX-Q as seen in Fig. 1. In 500 m*M* NaCl, however, when the electrostatic interaction responsible for binding at low ionic strength is shielded, BSA is almost completely excluded from the intraparticle space. For these conditions, BSA appears to behave in a manner similar to dextran T-40. In fact, these two molecules have a similar hydrodynamic radius of approximately 4 nm [18].

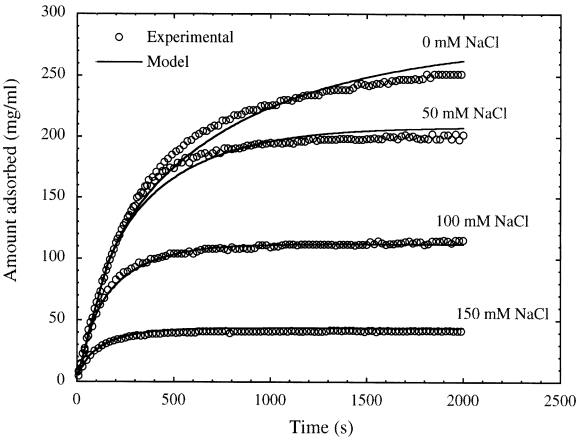

Fig. 3. Uptake curves for 1 mg/ml BSA in stirred-batch contactor in 50 m*M* Tris–HCl at pH 8.5 at different salt concentrations.

4.3. Adsorption and desorption kinetics

The effects of salt concentration on the adsorption of BSA are shown in Fig. 3 for experiments conducted in the stirred batch apparatus. The graph shows the amount of BSA adsorbed per ml of particle volume. As the salt concentration is increased, the amount adsorbed at equilibrium decreases. However, the time needed to reach equilibrium also decreases. As seen in Fig. 3, the initial portions of the uptake curves are nearly coincident for a substantial length of time. This result indicates that film mass transfer is the dominant resistance early on in the uptake process, even at high salt concentrations.

The effects of salt concentration on the desorption rate are shown in Fig. 4 for experiments conducted in the shallow-bed apparatus. The graph gives the amount of BSA desorbed per ml of particle volume at different salt concentrations. The initial BSA loading on the particles was 280 mg/ml for each case. As seen in this figure, desorption is essentially complete in about 200 s for both 200 and 500 m*M* NaCl, although the rate is somewhat lower for 200 m*M* NaCl. The initial rate of desorption is still fairly rapid for 100 and 50 m*M* NaCl. However, in this case, the rate slows down dramatically after the first 100–200 s. This behavior is explained by the fact that when the salt concentration is rapidly changed, a portion of the originally adsorbed protein diffuses

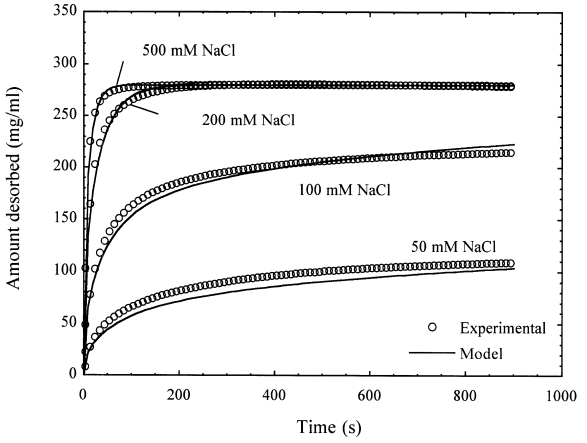

Fig. 4. Desorption curves for BSA in shallow-bed contactor in 50 m*M* Tris–HCl at pH 8.5 at different salt concentrations. Initial protein loading on BRX-Q = 280 mg/ml, $u = 1200$ cm/h.

rapidly out of the particle. Since at these lower salt concentrations, the isotherm is still quite favorable (see Fig. 1), the remaining portion of adsorbed protein is desorbed very slowly. As the system settles on the new isotherm at the lower salt concentration, the driving force for external mass transfer and, thus, the rate of desorption becomes extremely small.

In order to quantitatively compare mass transfer rates obtained for different conditions, we utilized the following model equations:

$$\frac{\partial q}{\partial t} = \frac{D_s}{r^2}\frac{\partial}{\partial r}\left(r^2\frac{\partial q}{\partial r}\right) \tag{2a}$$

$$t = 0, \quad q = q_0 \tag{2b}$$

$$r = 0, \quad \frac{\partial q}{\partial r} = 0 \tag{2c}$$

$$r = r_p,\ q = q_i, \quad D_s\frac{\partial q}{\partial r} = k_f(C - C_i) \tag{2d}$$

$$\frac{dC}{dt} = -\frac{V_M}{V}\frac{d\bar{q}}{dt} = -\frac{3k_f}{r_p}\frac{V_M}{V}(C - C_i) \tag{3a}$$

$$t = 0, \quad C = C_0 \tag{3b}$$

where q is the adsorbed protein concentration, D_s is an effective diffusivity, r_p is the particle radius, k_f is the boundary layer mass transfer coefficient, C and C_i are the protein concentration in the bulk fluid and at the particle surface, and V and V_M are the solution and particle volumes, respectively. In this model, we assume that the intraparticle mass transfer flux is proportional to the gradient in total protein concentration in the particle. Furthermore, we assume that at the fluid-particle interface q_i and C_i are related through the isotherm expression, Eq. (1), with parameters from Table 1 at each salt concentration. These equations were solved numerically by orthogonal collocation as described previously [19], and the solution was used to determine the effective diffusivity by fitting the experimental uptake curves. The same equations were also used to describe desorption in the shallow-bed by taking $V_M/V = 0$. The values of $k_f = 0.001$ and 0.002 cm/s, previously determined from low protein concentration experiments [17], were used for the stirred-batch and shallow-bed calculations, respectively. The resulting D_s-values are shown in Fig. 5 and calculated curves are shown in Figs. 3 and 4. The agreement between calculated and experimental data is good for both adsorption and desorption experiments. However, in each case, the diffusivity increases with salt concentration. Moreover, the diffusivities are different for adsorption and for desorption

The effect of salt concentration on the effective diffusivities can be explained as follows: For adsorption, as the salt concentration is increased, the attractive interaction between the negatively charged protein and the positively charged functional groups

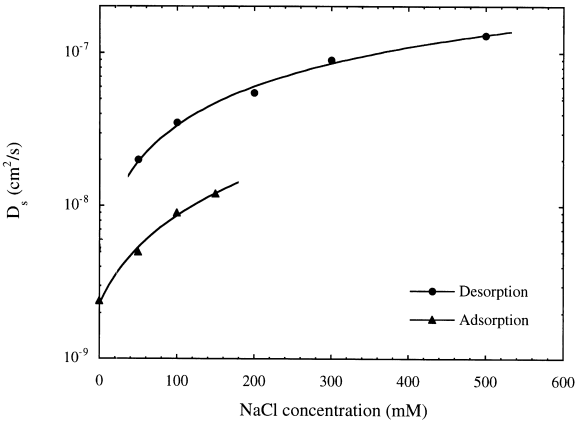

Fig. 5. Intraparticle diffusivities obtained from batch adsorption and shallow-bed desorption experiments at different salt concentrations.

is weakened. On one hand this can be expected to reduce the driving force for mass transfer while on the other it can be expected to increase the diffusional mobility. The situation is different for desorption. In this case, a large amount of protein is initially loaded on the particle. As the salt concentration is stepped up, salt diffuses rapidly within the particle creating a very large driving force for desorption. For these conditions a fraction of the pre-adsorbed protein becomes rapidly ''unbound'' and diffuses outwardly at a high rate. When desorption occurs at lower salt concentrations only a small fraction of the bound protein becomes free to diffuse unbound. As a result the effective diffusivity decreases. Conversely, at higher salt concentrations, most of the pre-adsorbed protein becomes unbound upon exposure to the salt solution. Thus, the entire amount of pre-adsorbed protein is rapidly desorbed virtually unhindered by the presence of the charged functional groups. It should be noted that while desorption from the particles at high salt concentrations is rapid, as discussed above, BSA remains essentially completely excluded from the particles if they are contacted with a protein solution containing 500 m*M* NaCl. This suggests that the polymer gel in BRX-Q has a flexible structure that allows the protein to diffuse out when pre-adsorbed at low salt and eluted with high salt, but that prevents the protein from diffusing in when starting at high salt.

It should be noted that a parallel diffusion model where free and bound protein forms are treated separately could also be considered as suggested, for example, by Yoshida et al. [3]. In principle, the contribution of free protein diffusion can be determined under non-binding conditions (e.g., at high salt concentrations). However, in our case, the protein is excluded from the particle under non-binding conditions, leading to the conclusion that free protein diffusion in the particle is near zero.

4.4. Breakthrough and elution behavior

Breakthrough curves for BSA on BRX-Q columns at different salt concentrations are shown in Fig. 6. The packed column length was 3.2 ± 0.1 cm, the mobile phase velocity was 300 cm/h, and the feed BSA concentration was 1 mg/ml. The column

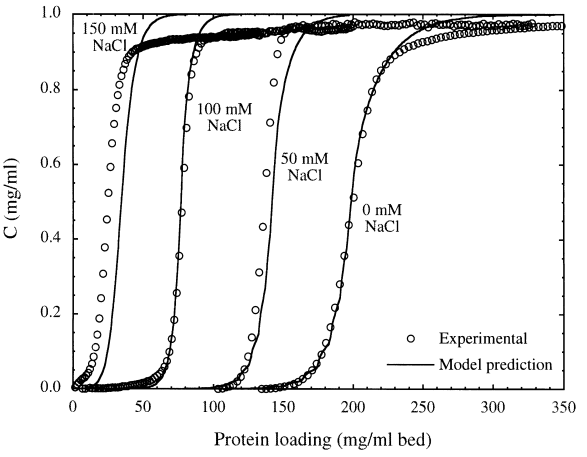

Fig. 6. Comparison of experimental and predicted breakthrough curves for 1 mg/ml BSA in 50 m*M* Tris–HCl buffer at pH 8.5 at different salt concentrations. Column length = 3.2 cm, $u = 300$ cm/h.

dynamic capacity decreases as the salt concentration is increased, as the isotherm becomes less favorable. However, the curves remain fairly sharp. For long times, each of the breakthrough curves exhibits a tailing behavior. This has been previously observed in several studies using BSA as a model protein (e.g., Refs. [8,17,20–22]). We determined that this tailing is caused by the presence of a small amount of strongly retained impurities in the feed, most likely a BSA dimer, which was estimated to be approximately 5% (as determined by ion-exchange and size-exclusion HPLC). To make this determination we first equilibrated a volume of BSA solution with a sample of BRX-Q. Since the BSA dimer is strongly adsorbed, the supernatant remained impurity-free. We then used the dimer-free solution to load a BRX-Q column. No severe tailing was observed in this case, demonstrating that the tailing is caused by the presence of small amounts of late-eluting, higher molecular mass impurities.

The breakthrough behavior at different salt concentrations was simulated using isotherm parameters from Table 1 and the D_s values obtained from batch uptake experiments. To make these predictions we used Eqs. (2a)–(2d) along with the following material balance and boundary conditions:

$$\epsilon_b \frac{\partial C}{\partial t} + (1 - \epsilon_b)\frac{\partial \bar{q}}{\partial t} + u\frac{\partial C}{\partial z} = 0 \qquad (4a)$$

$$t = 0, \quad C = C_0 \tag{4b}$$

$$z = 0, \quad C = C_F \tag{4c}$$

In these equations, ϵ_b is the extraparticle void fraction and u is the mobile phase superficial velocity. These equations were solved numerically as previously discussed [19]. Since mass transfer effects within these particles have been shown to be independent of mobile phase flow-rate [17], the parameters determined from the batch experiments should provide a suitable basis for predicting the column behavior, provided that flow conditions remain ideal. Predicted curves are shown in Fig. 6. In general, there is good agreement between experimental and predicted profiles. Although a slight deviation occurs in the breakthrough time at 150 m*M* NaCl, the slope of the breakthrough curve is correctly predicted. The model, of course, does not predict the extensive tailing behavior since it was based on measurements with the unpurified BSA. In turn, this causes a slight discrepancy in the prediction of the breakthrough curve at higher salt concentrations, where the presence of the BSA dimer has a more significant effect.

Fig. 7 shows the effluent protein concentration obtained from the UV detector signal during adsorption–elution cycles in a 1.75-cm long BRX-Q column (column volume = 0.34 ml) operated at 300 cm/h (1 ml/min). For each run we loaded 100 ml of a 1 mg/ml BSA solution in Tris buffer. At this loading level, the effluent concentration approaches 95% of the inlet value. After a 10-ml wash with Tris buffer, the column was eluted with different salt concentrations at 300 cm/h. Prior to each successive run the column was eluted with 500 m*M* salt to remove any residual adsorbed protein and then rinsed with buffer. As seen in this figure, the reproducibility of the breakthrough curves is excellent. However, reducing the eluent salt concentration below 500 m*M* significantly increases the time to achieve elution to baseline UV values. Below 200 m*M* NaCl, this time increases dramatically. For these conditions, elution is affected by the non-linear nature of the isotherm (see Fig. 1) and eventually becomes completely equilibrium controlled. Fractograms showing the complete elution profiles for these experiments are given in Fig. 8a and the corresponding protein recovery is given in Fig. 8b. Very high protein concentrations are obtained as the salt concentration is increased. At 500 m*M* NaCl, greater than 95% recovery is obtained in approximately 1.5 ml (or 1.5 min). This corresponds to approximately 4.4 column volumes. At 300 m*M* salt, 95% recovery is attained in approximately 4 ml, while at lower values of the NaCl concentration much longer times would be needed. The presence of some BSA dimer and, possibly, other impurities in the feed should, however, be noted as a complicating factor. Although an effect of salt concentration in the range of 300–500 m*M* salt is expected even for the monomer, it is likely that most of the difference was caused by these impurities.

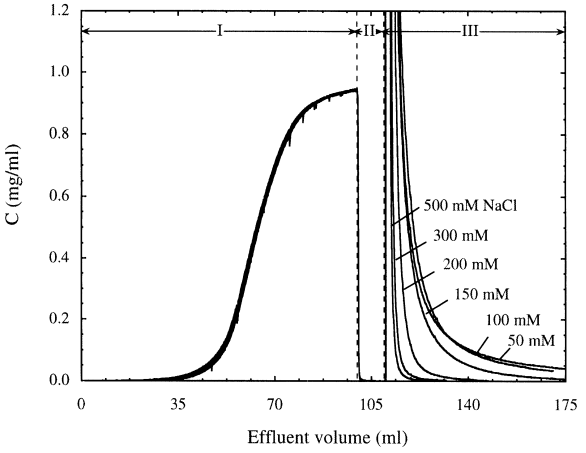

Fig. 7. Breakthrough and elution curves for BSA in a 1.75-cm column at 300 cm/h. (I) Feed load of 100 ml of 1 mg/ml BSA in 50 m*M* Tris–HCl; (II) wash with 10 ml Tris buffer; (III) elution with salt. Profiles obtained from UV detector signal.

The effect of eluent flow-rate is shown in Figs. 9 and 10. In each case, the column (1.75 cm long) was again loaded with 100 ml of a 1 mg/ml BSA solution in Tris buffer at 300 cm/h and then eluted with 500 m*M* NaCl. Fig. 9 shows the fractograms plotted both as a function of time and eluent volume. The insets in these figures show the protein concentrations derived from the UV signal below 1 mg/ml. As seen in these figures, while the eluent volume increases with flow-rate, the time needed to attain essentially full protein recovery and to approach baseline UV values decreases with flow-rate. In all cases, very high protein concentrations are

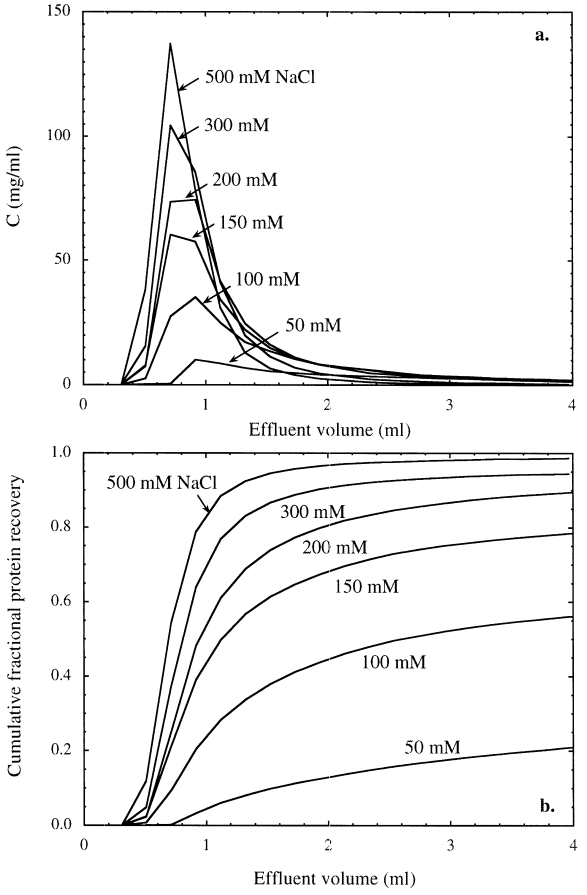

Fig. 8. Effect of salt concentration on elution at 300 cm/h: (a) elution peaks and (b) cumulative fractional protein recovery. Feed load = 100 ml of 1 mg/ml BSA, column length = 1.75 cm.

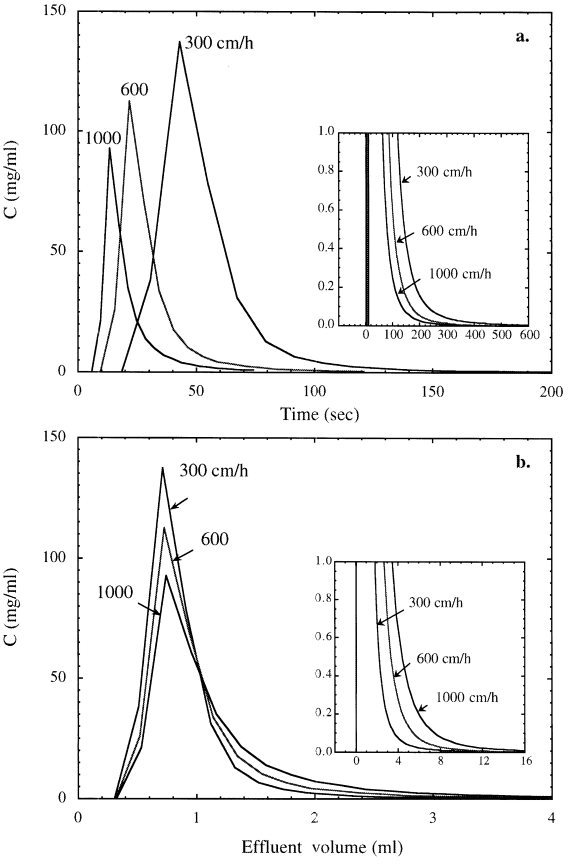

Fig. 9. Effect of flow-rate on elution with 500 m*M* NaCl: (a) effluent profiles vs. time and (b) effluent profiles vs. volume. Feed load = 100 ml of 1 mg/ml BSA, column length = 1.75 cm.

obtained in the fractions collected as a result of the high adsorption capacity of BRX-Q.

Fig. 10 shows the cumulative protein recovery values corresponding to the experiments in Fig. 9. As the flow-rate is increased, the eluent volume needed to recover 95% of the protein increases substantially. However, the time for desorption is substantially reduced. This may be advantageous as the cycle time can be shortened and the protein is recovered sooner. However, these data suggest that for an optimized cycle there will be a trade-off between cycle time and eluent consumption.

Fig. 11 provides a comparison of the elution profiles for a column (1.75 cm long) loaded with different amounts of BSA and eluted with 500 m*M* NaCl at 300 cm/h. In the first case, the column was loaded with 100 ml of 1 mg/ml BSA solution in Tris buffer at 300 cm/h while in the second case the loading was 52 ml. As noted above, the higher loading volume corresponds to 95% of breakthrough, while the lower value corresponds to 10% of breakthrough. As seen in this figure, the maximum protein concentration in the eluent decreases with the lower protein load. However, the eluent volume (and the time of elution) needed to achieve baseline UV values remains essentially unchanged.

The predictability of the elution behavior of the BRX-Q columns was tested by comparison with the model using the parameters determined from the

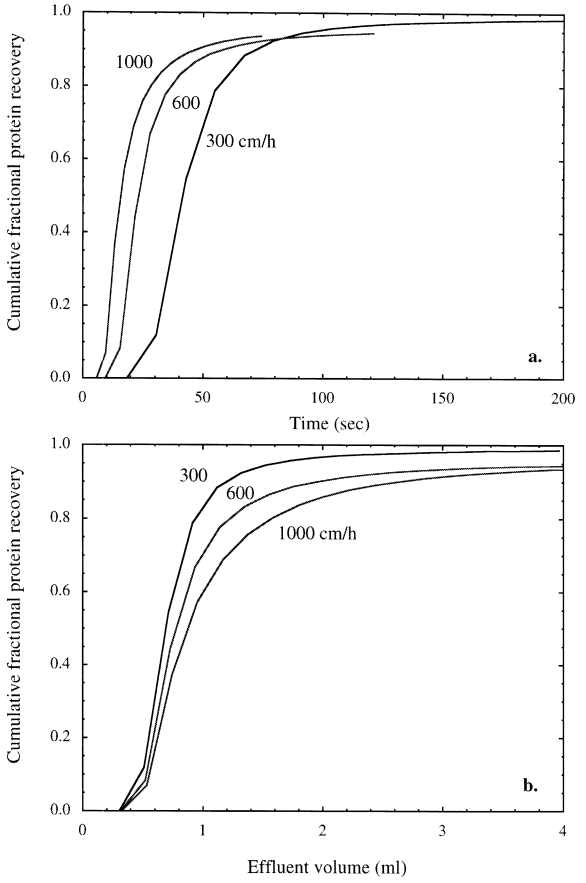

Fig. 10. Effect of flow-rate on protein recovery rate with 500 m*M* NaCl: (a) recovery vs. time and (b) recovery vs. volume. Conditions as in Fig. 9.

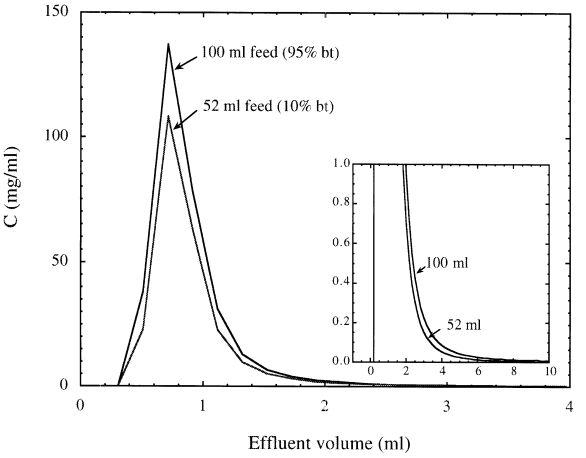

Fig. 11. Effect of protein load on elution profiles with 500 m*M* NaCl at 300 cm/h. Feed concentration = 1 mg/ml BSA, column length = 1.75 cm.

shallow-bed studies and the isotherm experiments. The model equations used to predict the breakthrough curves were also used to predict the elution behavior. In this case, the bed conservation equation [Eq. (4a)] was discretized by backward finite differences and the particle conservation equation by orthogonal collocation. The bed void fraction was estimated to be 0.31, based on a material balance accounting for the protein adsorbed at equilibrium, and is consistent with previously reported values for BRX-Q columns [17]. To simulate the movement of salt through the bed we assumed that salt moves as a sharp front at a constant velocity, v_s. This assumption is justified by the fact that in our experiments the salt in the elution buffer was in large molar excess over the protein. The value of v_s was determined by measuring experimentally the retention time of the salt front from the effluent conductivity. We found that $v_s = (1.16 \pm 0.02) \times u$. This value is in agreement with the retention volume determined from the pulse injections of NaCl shown in Fig. 2b. Thus, propagation of the salt through the column was simulated by changing equilibrium and rate parameters in a step-wise fashion to the values corresponding to the salt concentration upstream of the advancing front. The simulated results were ''binned'' in fractions with the same volume as the experimental fractions.

Fig. 12 shows a comparison of experimental and predicted fractograms for a 1.75-cm long BRX-Q column loaded with 1 mg/ml BSA and eluted with different salt concentrations at 300 cm/h. The previously determined value of $D_s = 2.4 \times 10^{-9}$ cm^2/s was used to simulate the adsorption in Tris buffer, while the diffusivity values given in Fig. 5, obtained from the shallow-bed experiments, were used for desorption. In general, the model is in good agreement with the experimental results. The worst case is elution with 50 m*M* NaCl. However, here the assumption of a perfectly sharp salt front may be questionable, which explains why the model fails to accurately predict the maximum concentration. Nevertheless, the model predicts the tailing behavior, which in this case is caused largely by the favorable nature of the isotherm.

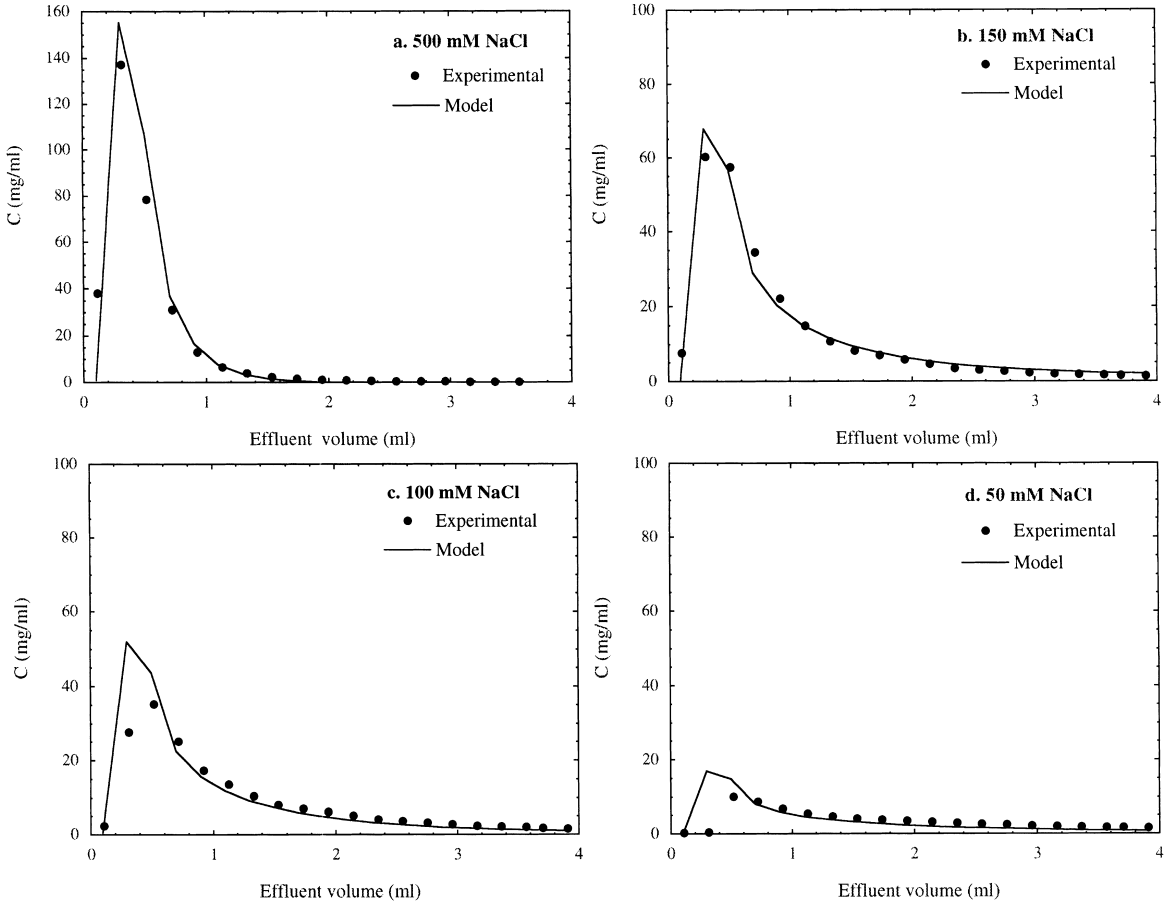

Fig. 12. Comparison of experimental and predicted elution profiles for BSA for 1.75-cm column at 300 cm/h with different salt concentrations. Experimental conditions as in Fig. 8. Model parameters from Table 1 and Fig. 5.

Fig. 13 shows a comparison of the experimental and predicted effects of the eluent flow-rate. As in the previous case, the diffusivities independently determined from the shallow-bed experiments were used in the simulations. In agreement with the experiments, the model predicts lower concentrations at higher flow-rates, but a faster time to attain a high recovery of the adsorbed protein.

Adsorption–desorption experiments were also conducted with a 10-cm long BRX-Q column (column volume = 1.96 ml) with a feed containing 5 mg/ml BSA in Tris buffer. The feed solution was supplied until 10% breakthrough. After a 10-ml buffer wash, the column was eluted with 500 m*M* NaCl. Fig. 14 shows the elution fractograms obtained for this longer column at different flow-rates plotted as a function of both time and eluent volume. As in the previous cases, the insets show the protein concentration determined from the UV signal in the range 0–1 mg/ml protein. As seen in this figure, a concentrated protein peak with some degree of tailing at very low concentrations is obtained. Most of the protein (>95%) is recovered in 4–6 ml. Thus, it appears that increasing column length does lengthen the time of elution dramatically. For the longer column, baseline UV values are attained after about 25–30 ml (25–30 min) at 300 cm/h and after about 40 ml (12.5 min) at 1000 cm/h.

Fig. 15 shows a comparison of predicted and experimental elution curves using the same parameters as before. The model predicts fairly accurately the elution fractogram at 1000 cm/h (Fig. 15b).

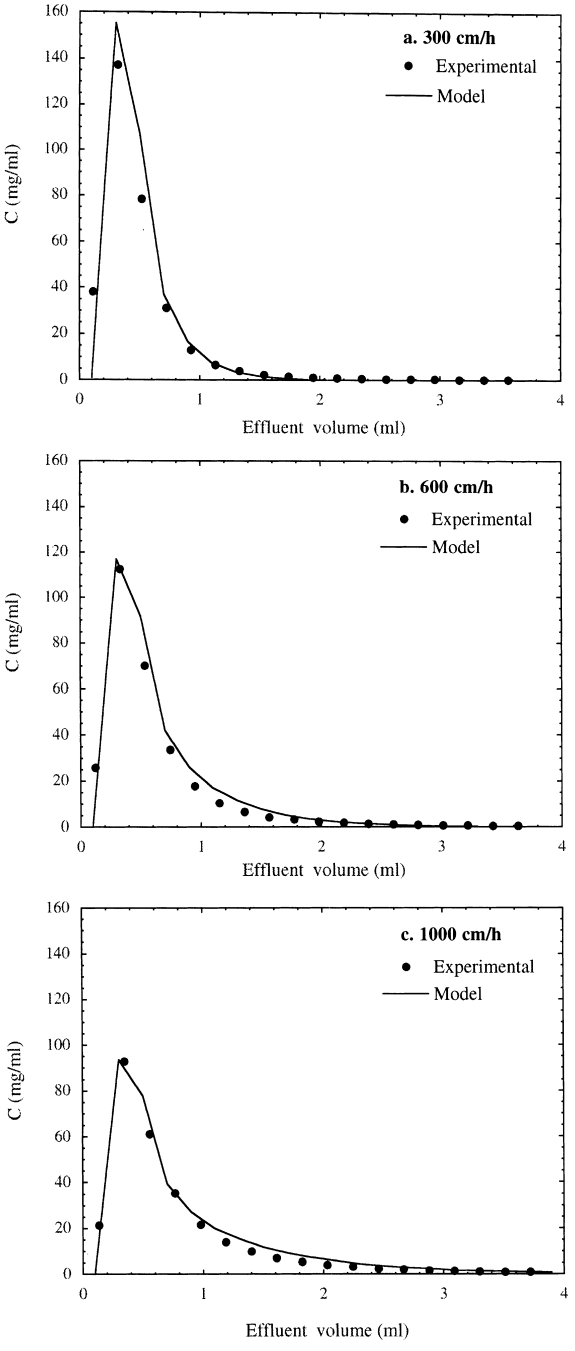

Fig. 13. Comparison of experimental and predicted elution profiles for BSA for 1.75-cm column with 500 m*M* salt at different flow-rates. Experimental conditions as in Fig. 9. Model parameters from Table 1 and Fig. 5.

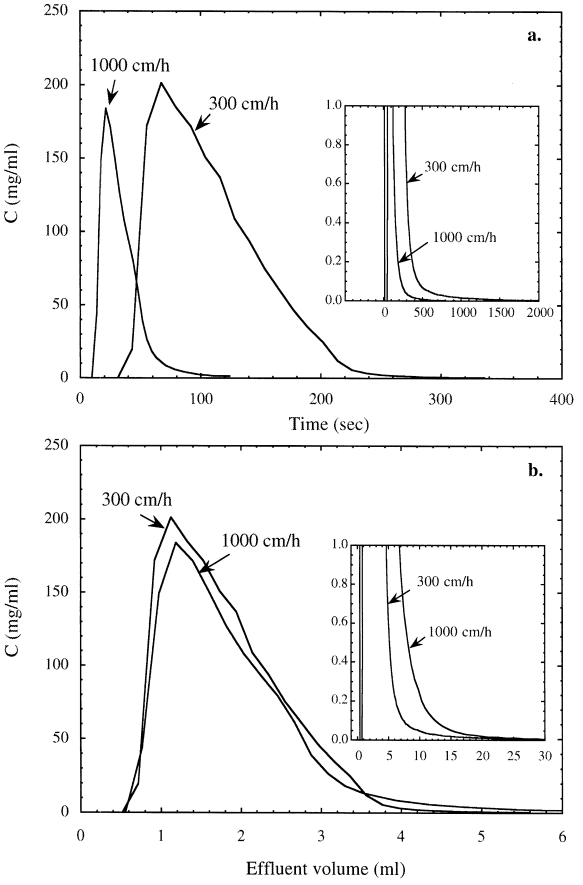

Fig. 14. Effect of flow-rate on elution with 500 m*M* NaCl: (a) effluent profiles vs. time and (b) effluent profiles vs. volume. Feed load = 5 mg/ml BSA to 10% breakthrough, column length = 10 cm.

However, significant deviations occur at 300 cm/h (Fig. 15a). The explanation for the discrepancy is likely viscous fingering. At 300 cm/h, the model predicts eluted fractions containing 300 mg/ml of BSA. The viscosity of such solutions would exceed 20 cp [23], or more than 20 times the viscosity of the eluent. This is likely to cause severe viscous fingering in the rear of the elution profile. For example, Yamamoto et al. [24] and Czok et al. [25] have observed severe viscous fingering effects under non-binding conditions at protein concentrations as low as 60 mg/ml, which is substantially lower than the protein concentrations attained in our work upon salt elution. Interestingly, the front of the elution profile appears to remain sharp, and, in fact, viscous finger-

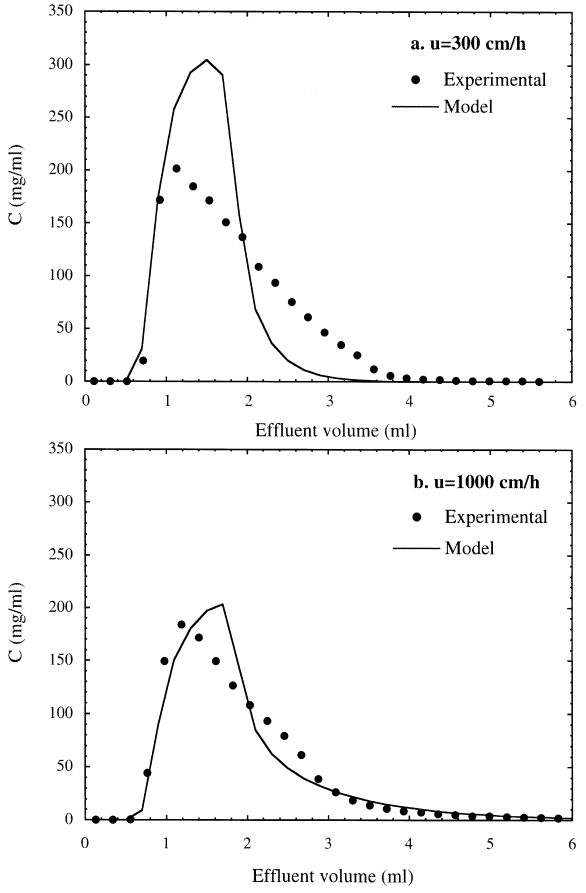

Fig. 15. Comparison of experimental and predicted elution profiles for BSA for 10-cm column with 500 m*M* salt at different flow-rates. Experimental conditions as in Fig. 14. Model parameters from Table 1 and Fig. 5.

ing is not expected to affect the leading edge of the elution profile in the same manner. Viscous fingering did not appear to have a strong effect on the higher flow-rate run or results obtained with the shorter columns. There are two principal reasons for this. Firstly, the maximum BSA concentration predicted for the eluted fractions is substantially lower, so that the viscosity would be lower. Secondly, the spreading of concentration bands by viscous fingering is dependent on residence time and is, thus, likely to be more severe for longer columns than for shorter ones and for columns operated at lower velocities. Several ways of controlling the eluted protein concentration can be considered. For example, lower protein concentrations can be obtained with multiple step elution with increasing salt concentrations or with linear gradient elution.

4.5. Productivity considerations

The productivity for a cyclic adsorption–elution operation can be defined as follows:

$$P = \frac{\text{amount of protein recovered}}{\text{column volume} \times \text{processing time}} \quad (5)$$

where P is defined for a given percent of breakthrough, say 10%. In practice, the processing time comprises, as a minimum, four contributions: feed load time, wash time, elution time, and re-equilibration time [10]. The time for a clean-in-place step may also have to be considered. However, for simplicity, here we consider only feed load and elution times since wash and re-equilibration times are fairly short. Dynamic binding capacity (DBC) is also often used as a measure of performance. The latter is calculated as the amount of protein adsorbed per unit column volume when the effluent reaches 10% of the feed concentration.

Fig. 16 shows the effects of superficial velocity on DBC and the productivity. The experimental elution times needed to attain baseline UV values were used to calculate the productivity. In the first case, shown in Fig. 16a, we kept the elution velocity constant at 300 cm/h, while in the second, shown in Fig. 16b, the elution velocity was the same as the loading velocity. It can be seen that in both cases the productivity increases with feed mobile phase velocity. However, the increase in productivity is more pronounced if the elution velocity is also increased. Model predictions of the productivity were also made based on the predicted breakthrough behavior and the experimentally determined elution time. In both cases, the model predictions are in good agreement with the experimental results. It should be noted, however, that the time of elution used in these calculations is probably unnecessarily long since most of the adsorbed protein is in fact recovered in a much shorter time, as shown by the fractograms in Fig. 14. Thus, the productivity values shown in Fig. 16 are lower bound estimates. Moreover, no attempt was made to optimize productivity, which could be done by systematically varying the column length and flow-rates. Thus, these productivity data are

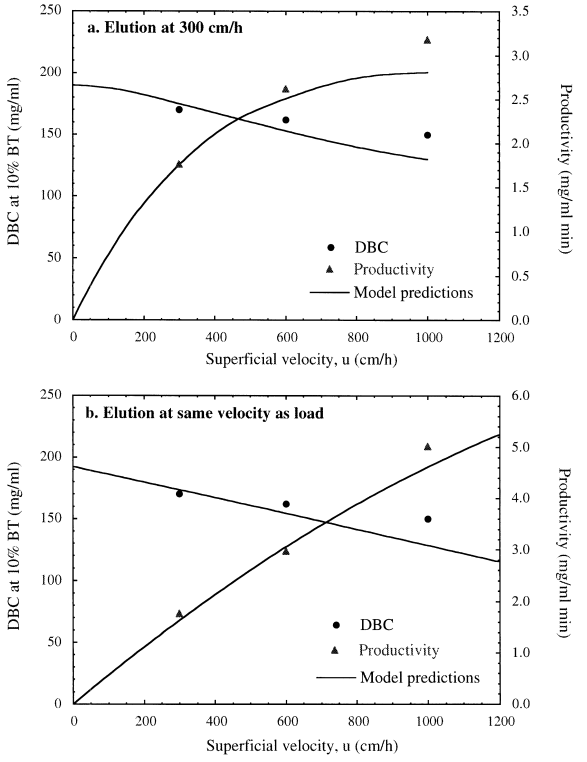

Fig. 16. Comparison of experimental and predicted dynamic binding capacity (DBC) at 10% breakthrough and productivity for 10-cm column as a function of loading mobile phase velocity: (a) elution at 300 cm/h and (b) elution at same velocity as load velocity. Feed load = 5 mg/ml BSA, eluent = 500 m*M* NaCl.

given only to illustrate the general trends of DBC and productivity as a function of mobile phase velocity.

5. Conclusions

We have studied the effects of salt on the adsorption and desorption of BSA on BRX-Q, an acrylamido-based anion-exchanger. This material possesses a heterogeneous gel structure that is sufficiently rigid to allow column operation at fairly high flow-rates, while retaining a high adsorption capacity. In the absence of an attractive interaction, macromolecules are nearly completely excluded from the intraparticle space of this material. However, negatively charged proteins are strongly bound at low salt concentrations and are eluted quantitatively at high concentrations. The adsorption capacity for BSA decreases as the salt concentration is raised. However, both adsorption and desorption rates increase as the salt concentration is increased. This behavior is attributed to the fact that the protein mobility in the gel increases as the attractive interaction with the functional groups of the media is shielded by the salt. Effective diffusivities based on a homogeneous diffusion model were obtained for adsorption and desorption of BSA at different salt concentrations from batch and shallow-bed experiments. The model, in conjunction with the experimentally determined diffusivities, provides a good prediction of the elution behavior of packed columns with different lengths, mobile phase velocities, protein feed concentrations, and salt concentrations. As a result of the high equilibrium adsorption capacity and mass transfer rates of BRX-Q, high dynamic capacities, high productivity, and highly concentrated product fractions can be obtained even in very short columns. The experimental approach and model developed in this work provide the means for the determination of optimum operating conditions.

6. Nomenclature

b	Adsorption isotherm parameter (ml/mg)
C	Protein concentration in solution (mg/ml)
C_F	Feed protein concentration (mg/ml)
C_0	Initial protein concentration in solution (mg/ml)
C_i	Protein concentration in solution at particle-fluid interface (mg/ml)
D_s	Effective diffusivity (cm^2/s)
k_f	External film mass transfer coefficient (cm/s)
P	Productivity (mg/ml min)
q	Protein concentration in particle (mg/ml)
q_i	Protein concentration in particle at particle-fluid surface (mg/ml)
q_m	Adsorption isotherm parameter (mg/ml)
q_0	Initial adsorbed protein concentration (mg/ml)
$\bar{q}$	Average concentration in particle (mg/ml)

r	Particle radial coordinate (cm)
r_p	Particle radius (cm)
t	Time (s)
u	Mobile phase superficial velocity (cm/s)
v_s	Velocity of propagation of salt front through bed (cm/s)
V	Solution volume (ml)
V_c	Column volume (ml)
V_e	Eluted volume (ml)
V_M	Volume of adsorbent particles (ml)
z	Bed length coordinate (cm)
ϵ_b	Extraparticle void fraction

Acknowledgements

This research was supported by Bio-Rad Laboratories, Inc., and by NSF Grant No. CTS-0079334.

References

[1] E.N. Lightfoot, Ind. Eng. Chem. Res. 38 (1999) 3628.
[2] G.L. Skidmore, B.J. Horstmann, H.A. Chase, J. Chromatogr. 498 (1990) 113.
[3] H. Yoshida, M. Yoshikawa, T. Kataoka, AIChE J. 40 (1994) 2034.
[4] G.F. Bloomingburg, G. Carta, Chem. Eng. J. 55 (1994) B19.
[5] M.A. Fernandez, W.S. Laughinghouse, G. Carta, J. Chromatogr. A 746 (1996) 185.
[6] L.E. Weaver Jr., G. Carta, Biotechnol. Progr. 12 (1996) 342.
[7] C. Chang, A.M. Lenhoff, J. Chromatogr. A 827 (1998) 281.
[8] K. Miyabe, G. Guiochon, Biotechnol. Progr. 15 (1999) 740.
[9] S. Yamamoto, K. Nakanishi, R. Matsuno, Ion Exchange Chromatography of Proteins, Marcel Dekker, New York, 1988.
[10] G. Sofer, L. Hagel, Handbook of Process Chromatography: A Guide To Optimization, Scale-up and Validation, Academic Press, New York, 1997.
[11] E.E. Graham, C.F. Fook, AIChE J. 28 (1982) 245.
[12] H. Tsou, E.E. Graham, AIChE J. 31 (1985) 1959.
[13] R.K. Lewus, F.H. Altan, G. Carta, Ind. Eng. Chem. Res. 37 (1998) 1079.
[14] J.R. Conder, B.O. Hayek, Biochem. Eng. J. 6 (2000) 225.
[15] R.K. Lewus, G. Carta, J. Chromatogr A 865 (1999) 155.
[16] A.K. Hunter, G. Carta, J. Chromatogr. A 897 (2000) 65.
[17] A.K. Hunter, G. Carta, J. Chromatogr. A 897 (2000) 81.
[18] P.G. Squire, J. Chromatogr. 210 (1981) 433.
[19] M.S. Saunders, J.B. Vierow, G. Carta, AIChE J. 35 (1989) 53.
[20] A.E. Rodrigues, J.M. Loureiro, C. Chenou, M. Reundeles de la Vega, J. Chromatogr. B 664 (1995) 233.
[21] E. Hansen, J. Mollerup, J. Chromatogr. A 827 (1998) 259.
[22] G. Iberer, R. Hahn, A. Jungbauer, LC–GC 17 (1999) 999.
[23] K. Monkos, Int. J. Biol. Macromol. 18 (1996) 61.
[24] S. Yamamoto, M. Nomura, Y. Sano, J. Chem. Eng. Japan 19 (1986) 227.
[25] M. Czok, A.M. Katti, G. Guiochon, J. Chromatogr. 550 (1991) 705.